Electronic Supplementary Material (ESI) for Nanoscale Advances.

Electronic Supplementary Information

First-Principles Calculations on Monolayer WX_2 (X = S, Se) as an Effective Drug Delivery Carrier for Anti-Tuberculosis Drugs

Khaled Mahmud, Taki Yashir and Ahmed Zubair*

Department of Electrical and Electronic Engineering, Bangladesh University of Engineering and Technology, Dhaka 1205, Bangladesh

E-mail: ahmedzubair@eee.buet.ac.bd

S1 Site Dependency of Adsorption Energy

We calculated adsorption energy for different adsorption sites of INH drug-absorbed WS_2 nanosheet. We considered three new configurations: hydrogen (H) atoms are near to 2D TMD nanosheet, oxygen (O) atom is near, and nitrogen (N) atom is closer. In Figure S1, we can see newly considered orientations. We compared the adsorption energies of three additional configurations with our reported structure in the manuscript.

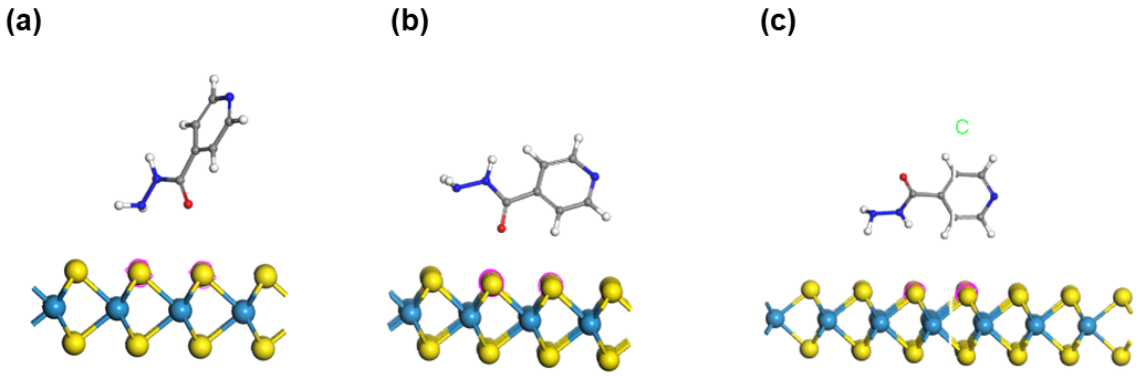

Figure S1: Configurations of INH/WS_2 with (a) H atoms, (b) O atom, and (c) N atom of INH near the WS_2 nanosheet.

Table S1: Adsorption energies when INH drug was absorbed on WS2 nanosheet in different orientations

Configurations (INH/WS_2)	Adsorption Energy (eV)
When H atoms are near	-0.52
When O atom is near	-0.66
When N atom is near	-0.41 eV
Our reported structure (when drug was adsorbed almost parallel to the nanosheet)	-0.96 eV

From Table S1, it is evident that our reported structure was the most stable one. It can be noted that, when the drug structure is parallel to the 2D nanosheet, it is more probable to get lower adsorption energy.

S2 Optical Calculation

We analyzed the optical characteristics for geometrically optimized drug complexes utilizing the CASTEP tools in Materials Studio. The energy range was 10 ev, employing a (5×5×1) k-point set with a band energy tolerance of 10^{-5} eV. GGA PBE functionals were applied, and smearing was set to 0.1 eV. The simulation involved passing polarized light through the drug complexes, followed by the calculation and plotting of the absorption coefficient against frequency. The absorption coefficient was determined by evaluating the imaginary component of the complex dielectric function. The imaginary portion of the dielectric function, represented as ε_2, was computed by summing across conduction bands using the technique outlined in the suggested method ,[1]

$$\varepsilon_2\left(\mathbf{q} \rightarrow O_{\hat{u}}, \hbar\omega\right) = \frac{2e^2\pi}{\Omega\varepsilon_0} \sum_{\mathbf{k},\nu,c} \left|\langle\Psi_{\mathbf{k}}^c|\mathbf{u}\cdot\mathbf{r}|\Psi_{\mathbf{k}}^\nu\rangle\right|^2 \delta\left(E_{\mathbf{k}}^c - E_{\mathbf{k}}^\nu - \hbar\omega\right) \tag{1}$$

Here, $\mathbf{u}$ represents the vector that defines the polarization of the incident light, and $|\langle\Psi_{\mathbf{k}}^c|\mathbf{u}\cdot\mathbf{r}|\Psi_{\mathbf{k}}^\nu\rangle|$ denotes the matrix element. The energies of the conduction band and valence band at wave number k are denoted as $E_{\mathbf{k}}^c$ and $E_{\mathbf{k}}^v$, respectively. The charge of an electron is represented by e, ω stands for angular frequency, $\hbar$ is the reduced Planck's constant, $\mathbf{u}.\mathbf{r}$ is the momentum operator, and Ω represents the crystal volume. The real part, ε_1, was determined through the Kramers-Kronig transformation[2] as given by,

$$\varepsilon_1(\omega) = 1 + \frac{2}{\pi} P \int_0^\infty \frac{\varepsilon_2\left(\omega^*\right)\omega^*}{\omega^{*2} - \omega^2}\, \mathrm{d}\omega^* \tag{2}$$

In this context, P denotes the principal value of the integral. The complex refractive indices, n and κ, are linked to the dielectric functions through the following expressions,

$$\begin{aligned} \varepsilon_1(\omega) &= n^2 - \kappa^2 \\ \varepsilon_2(\omega) &= 2n\kappa \end{aligned} \tag{3}$$

The relation between the absorption coefficient, denoted as α, and the imaginary and real dielectric constants is expressed as follows,

$$\alpha(\omega) = \frac{4\pi\kappa(\omega)}{\lambda} = \frac{4\pi}{\lambda\sqrt{2}} \left(\sqrt{\varepsilon_1^2(\omega) + \varepsilon_2^2(\omega)} - \varepsilon_1(\omega) \right)^{1/2}. \quad (4)$$

Here, κ denotes the extinction coefficient, and λ represents the wavelength.

S3 Projected density of states of drug atoms

In our comprehensive analysis, we extended our investigation to include a detailed examination of the partial density of states (PDOS) for each atom type within the drug complexes. The insights gained from these analyses shed light on the orbital contributions of individual atoms, providing a nuanced understanding of their electronic behavior. Figures S2 (a)-(d) show the calculated PDOS of individual drug atoms in INH/PZA(H)/WS_2. Figures. S3 (a)-(d) shows the similatar results for INH/PZA(H)/WSe_2 structure.

For INH/PZA(H)/WS_2 structure, our findings revealed that the DOS predominantly comprised p orbitals. P orbitals of nitrogen and oxygen contributed substantially in the vicinity of the band edges. On the other hand, p orbitals of carbon atoms contributed, particularly extending deep into both the conduction and valence bands. The structural configuration of INH/PZA(H)/WSe_2 exhibited a comparable pattern. The presence of p orbitals predominantly characterized the density of states (DOS) in this context. In proximity to the band edges, noteworthy contributions to the p orbitals arose from nitrogen and oxygen. Furthermore, the p orbitals of carbon atoms contributed significantly, extending deeply into both the conduction and valence bands.

A distinctive feature of the DOS was the minimal presence of s orbitals, with their contribution being marginal compared to the prevalent p orbitals. This minor orbital contribution was mainly attributed to the presence of hydrogen and nitrogen atoms within the drug's molecular structure. Notably, the s orbitals of nitrogen atoms involved much more than

hydrogen atoms' s orbital contribution in the valance band. The preeminent contributor to the density of states was the p orbital of nitrogen in both bands, emphasizing its substantial influence on the electronic structure. However, the p orbital of carbon atoms dominated in both bands, with the contribution from the s orbital deemed inconsequential.

Intriguingly, our analysis indicated that the contribution of s orbitals of oxygen in the valance band was even lower than that of hydrogen, nitrogen, and carbon atoms. Nevertheless, similar to nitrogen, the p orbitals of oxygen atoms played a pivotal role in shaping the overall states, underscoring its significance in the electronic structure of the drug complexes. One main notable difference was that drug atoms had larger contributions in WS_2 drug complex in comparison to WSe_2 close to the valance band maxima (VBM) and conduction band minima (CBM).

This detailed examination of the partial density of states offers a nuanced perspective on the electronic contributions of each atom type within the drug complexes, enriching our understanding of their electronic properties and potential implications for the compounds' behavior and reactivity. These insights contribute valuable information for the rational design and optimization of drug molecules with targeted electronic properties.

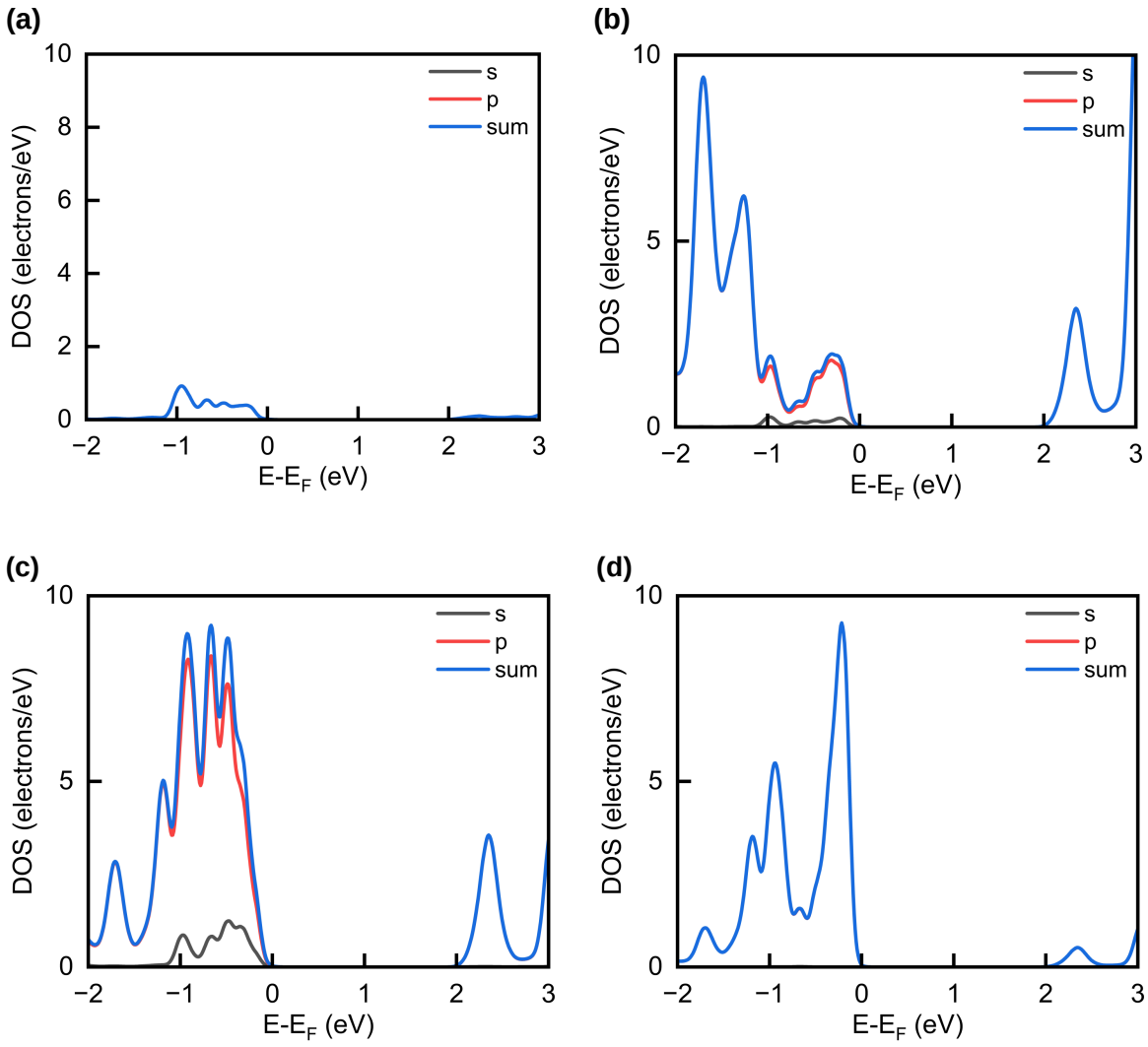

Figure S2: PDOS of (a) H atoms, (b) C atoms, (c) N atoms, and (d) O atoms for INH/PZA(H)/WS_2.

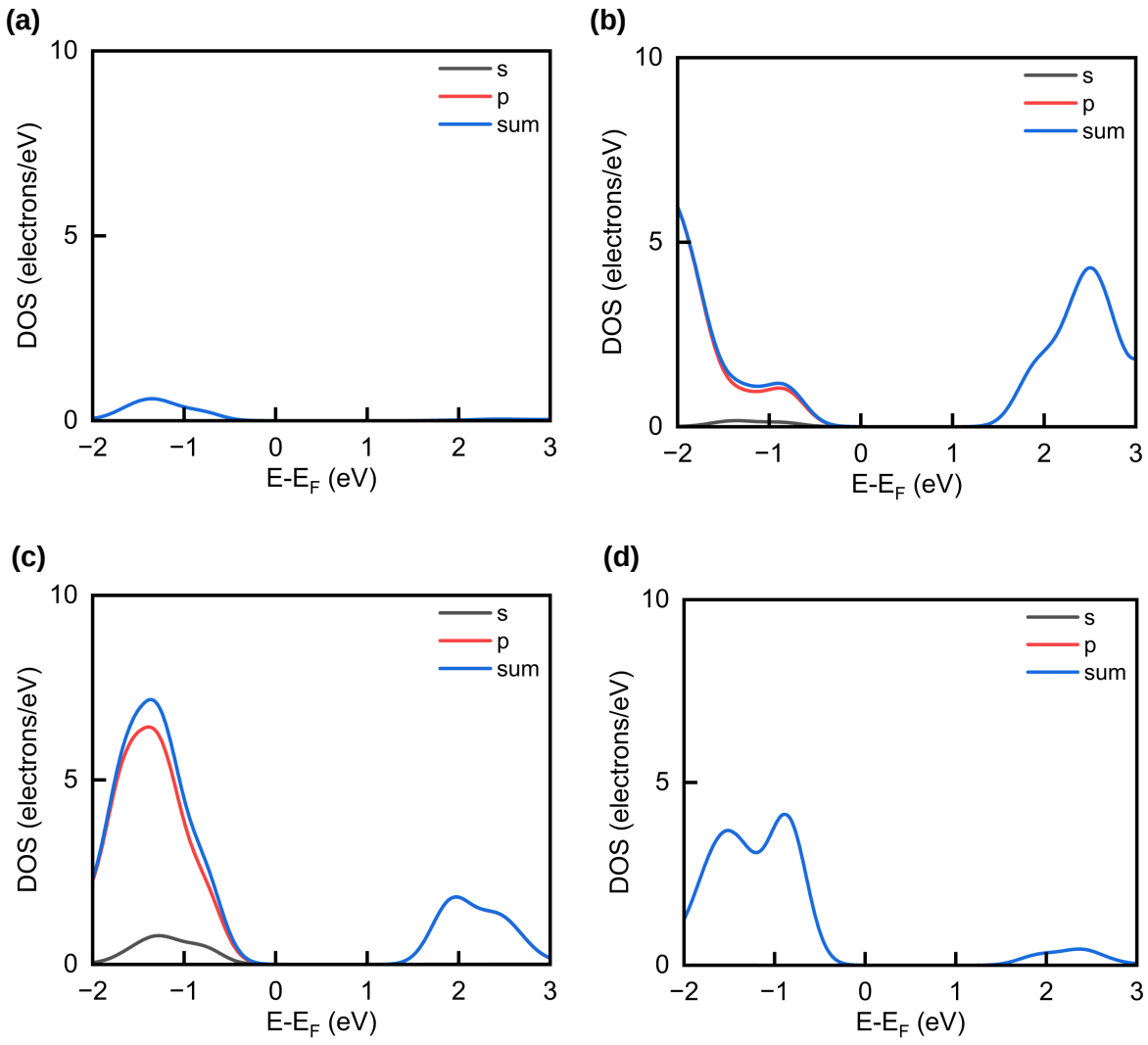

Figure S3: PDOS of (a) H atoms, (b) C atoms, (c) N atoms, and (d) O atoms for INH/PZA(H)/WSe_2.

S4 PDOS of pristine monolayer WS_2 and WSe_2 structures

In our comprehensive analysis, we extended our investigation to include a detailed examination of PDOS for pristine 2D TMD sheets (WS_2 and WSe_2). Figure S4 shows the PDOS of pristine WS_2 and WSe_2. The insights gained from these analyses shed light on the orbital contributions of the atoms, providing a nuanced understanding of their electronic behavior.

In the context of the WS_2 structure, it was found that the d orbital primarily dominated the overall states. Following closely, the p orbital emerged as the second-largest contributor to the DOS. Conversely, there was no significant contribution from the f orbitals to the DOS. Interestingly, a similar pattern of contributions was observed in the WSe_2 structure, underscoring similarities in the electronic behavior of these two distinct TMD sheets. This detailed examination of the PDOS for pristine 2D TMD sheets enhanced our understanding of the electronic characteristics of WS_2 and WSe_2, providing crucial insights that contribute to the broader understanding of their electronic structure and potential applications in various fields, including materials science and nanotechnology.

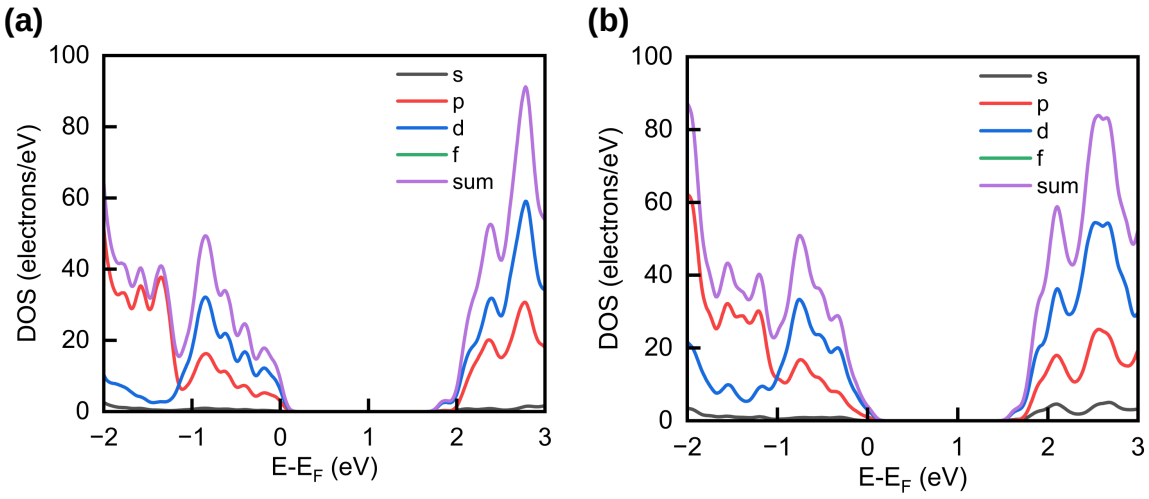

Figure S4: PDOS of (a) WS_2, and (b) WSe_2.

S5 Electronic band structures of WS_2 and WSe_2 monolayers by HSE06 functionals

We calculated band structures of monolayer WS2 and WSe2 with HSE06 hybrid functional to compare our calculations with previously reported experimental results.

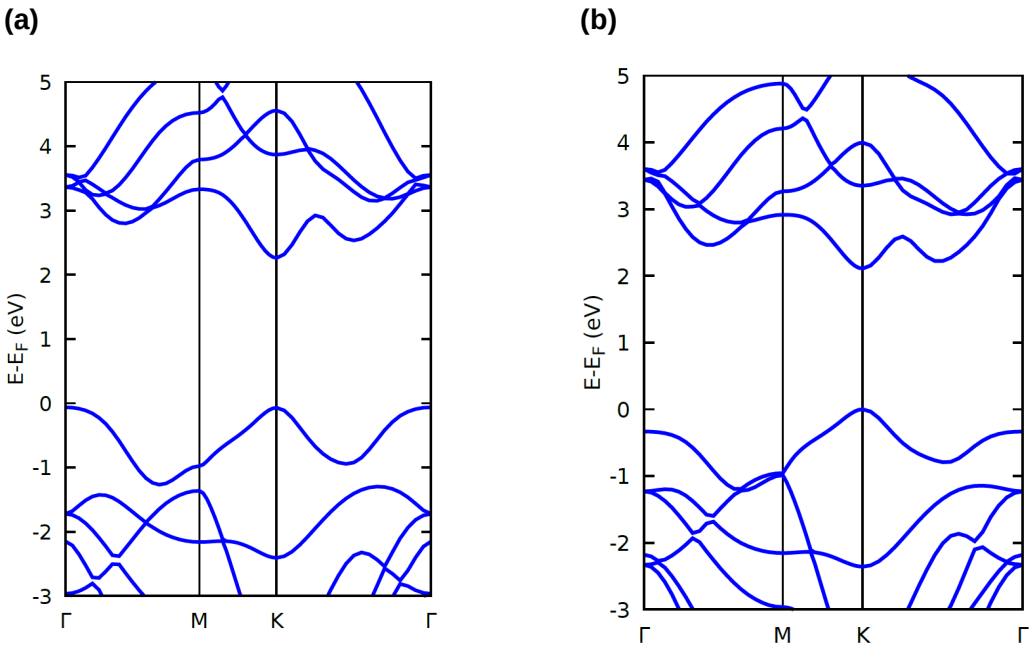

Figure S5: Band structures of (a) WS_2, and (b) WSe_2 with HSE06 hybrid functional.

From Figure S5 we can see the band structures of two TMD monolayers. For WS_2 monolayer, the calculated bandgap was 2.34 eV, whereas for WSe_2 monolayer, the bandgap was 2.15 eV.

S6 Electronic band structures of INH(V)/2D TMD

We conducted an analysis of the electronic band structures for vertical orientations, specifically focusing on INH(V)/WS_2 and INH(V)/WSe_2. Figure S6 illustrates the electronic band structures and corresponding DOS of these configurations. Upon close examination, it became evident that the electronic band structures for vertical orientations closely resembled those observed in horizontal orientations.

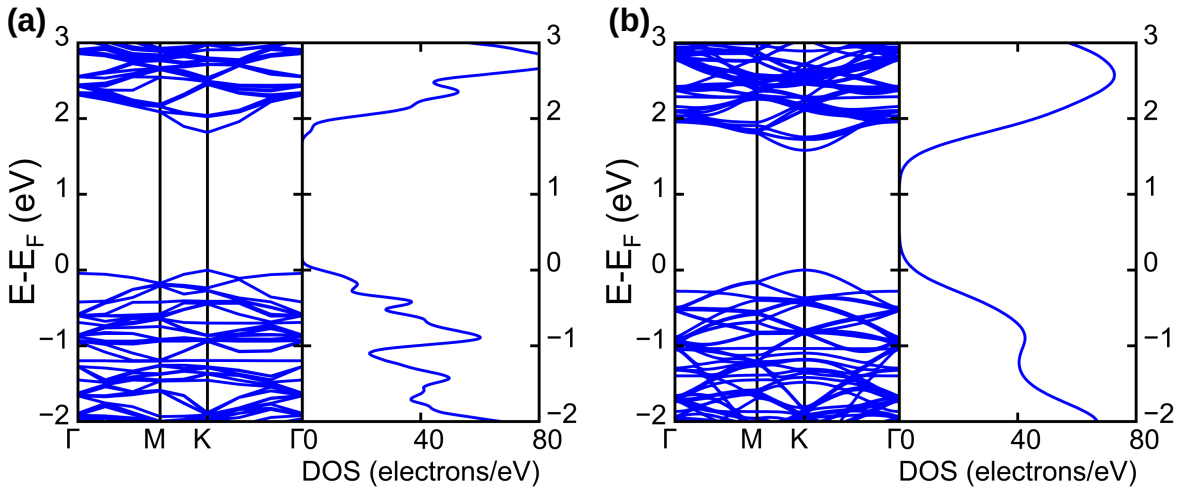

Figure S6: Electronic band structures of (a) INH(V)/WS_2, (b) INH(V)/WSe_2.

The bandgap of INH(V)/WS_2 and INH(V)/WSe_2 are 1.81 eV and 1.58 eV respectively. These bandgaps in both orientations were very close to their respective pristine and horizontal structures. Notably, both vertical orientations had direct bandgap, mirroring the behavior observed in the pristine TMDs. This analysis enhanced our understanding of the electronic characteristics of INH(V)/WS_2 and INH(V)/WSe_2 in vertical orientations, providing valuable insights into their band structures and reinforced the significance of the d orbital in influencing electronic properties, particularly near the bandgap.

S7 Molecular Orbitals

We calculated the molecular orbitals for two of the most energetically favorable structures when INH and PZA drugs are adsorbed on 2D TMD surfaces. In Figure S7, (a) and (b) represent the highest occupied molecular orbital (HOMO) for INH/PZA/WS2 and INH/PZA/WSe2, and (c), (d) represent the lowest unoccupied molecular orbitals for the same structures. The figures show that no chemical bond is formed between the drug structures and 2D TMD sheets.

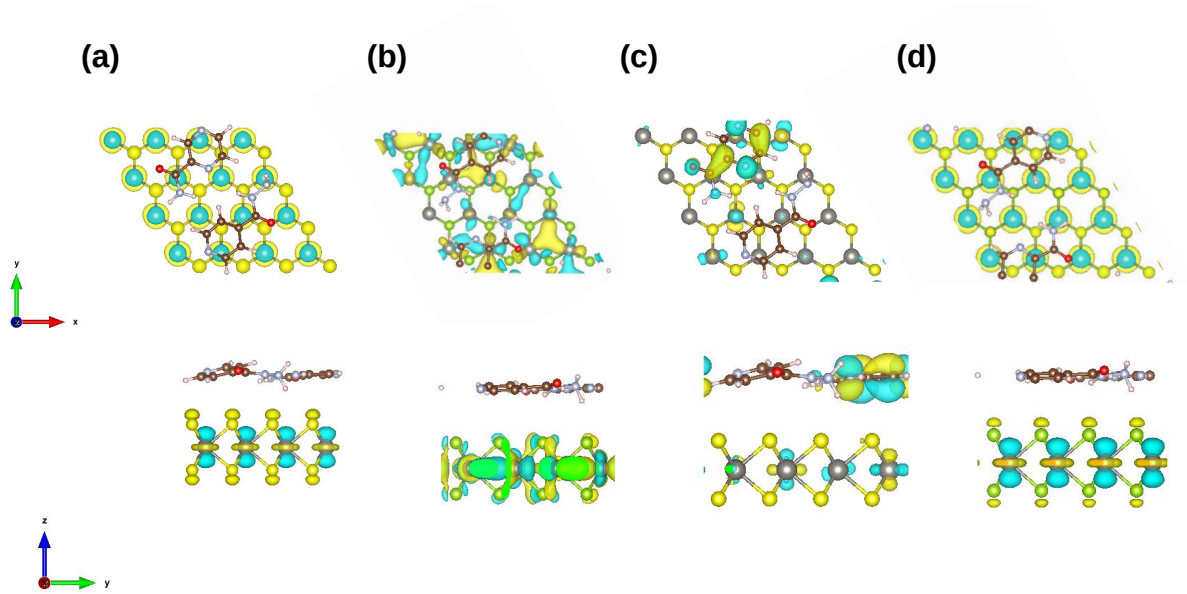

Figure S7: Top and side views of HOMO of (a) INH/PZA/WS_2 and (b) INH/PZA/WSe_2, and LUMO of (c) INH/PZA/WS_2 and (d) INH/PZA/WSe_2.

S8 Electron Localization Function (ELF)

We calculated and plotted electron localization function (ELF) for two of the most energetically favorable structures when INH and PZA drugs simultaneously adsorbed on 2D nanosheets. Figure S8 (a) shows the ELF for INH/PZA/WS_2 structure and (b) shows the ELF for INH/PZA?WSe_2. The ELF calculated figures suggest that no chemical bond formed between drug atoms and 2D nanosheet rather the adsorption process was a physisorption process. However, we can see a strong interaction between the atoms of 2D TMD sheets.

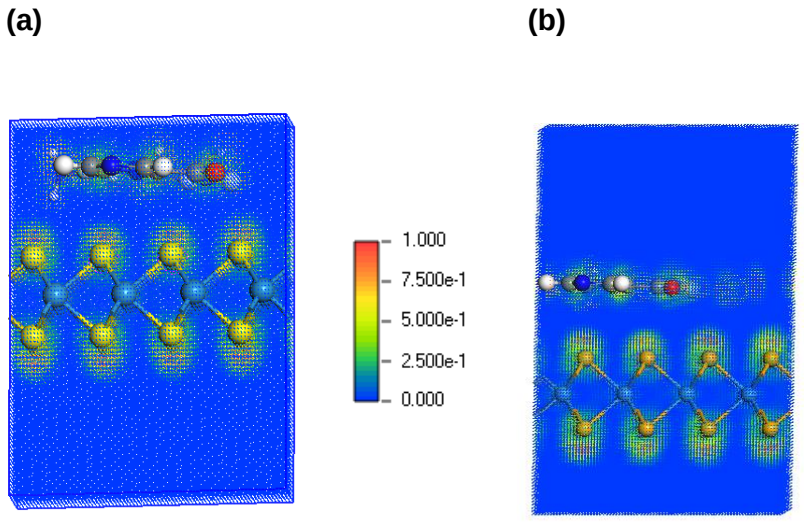

Figure S8: Plotted electron localization function (ELF) for (a) INH/PZA/WS_2, (b) INH/PZA/WSe_2. Here, the blue color (0) means no bond is formed, and the red color (1) means a strong bond is formed between the atoms.

References

(1) Gajdoš, M.; Hummer, K.; Kresse, G.; Furthmüller, J.; Bechstedt, F. Linear optical properties in the projector-augmented wave methodology. *Physical Review B* **2006**, *73*, 045112.

(2) Palik, E. D. *Handbook of optical constants of solids*; Academic press, 1998; Vol. 3.